SHEAR MOMENT INTERACTION IN CONFINED MASONRY WALLS

A. Manzano[1] and J.J. Perez-Gavilan[2]

[1] PhD. Student, Instituto de Ingeniería de la UNAM, Av. Universidad 3000, Ciudad Universitaria, CP 04510, México, D.F., AManzanoT@iingen.unam.mx

[2] Researcher, Instituto de Ingeniería de la UNAM, Av. Universidad 3000, Ciudad Universitaria, CP 04510, México, D.F., JPerezGavilanE@iingen.unam.mx

ABSTRACT

Using as *a priori* hypothesis that drift is the main cause of first inclined cracks due to tension, a cracking shear strength prediction for earthquake resistance confined masonry walls is proposed as a function of flexural moment on its top. The prediction is relative to the nominal cracking shear strength when no flexural moment is present on top of the wall. To verify the developed expression, an experimental program was conducted in which four full-scale confined masonry walls were tested, two of them using hand-made solid clay bricks and two using extruded clay multi-perforated bricks. The first wall of each set, subjected to cyclic lateral loads only, was used as reference. The second wall in each set was loaded with cyclic shear force and flexural moment. A reduction of the cracking shear force was observed in the second wall as expected and in good agreement with the prediction. Other observed differences are also described.

KEYWORDS: confined masonry, interaction, shear strength, flexure, predicted strength, masonry walls

INTRODUCTION

Confined masonry is extensively used in many countries in Latin America, including México, Peru, Chile etc., the Middle East, East Europe and south Asia [1]. One of the main characteristics of the system is its sequence of construction. The wall is built first, with masonry units joined with mortar in running bond pattern. Once the wall is constructed small reinforced concrete tie-columns and tie-beams are cast in place to confine the wall. To increase its shear strength, horizontal reinforcement may be embedded in the mortar joins and anchored in the tie-columns [2]. For a complete description and practice refer to Confined Masonry Network [3].

Extensive tests have demonstrated that when built and detail adequately walls may have reasonable levels of displacement capacity and of shear, flexural and axial resistance [4]. Up to date this structural system is used for relatively low rise buildings: in México up to five floors and in other countries is restricted to one or two floor houses [5], [6]. Accordingly, experiments have been conducted mainly with walls subjected to different levels of axial and a lateral loads with no direct application of flexural moment on top of the wall, as in low rise buildings its magnitude and effect is considered small compared to shear.

Influence of flexural moment on shear cracking resistance has been associated to slenderness of the wall using the shear span ratio as parameter M/VL which can be interpreted as an effective aspect ratio H_e/L with $H_e = M/V$. Several authors [7], [8], [9], [10], [11], [12] have referred to the effect of aspect ratio in shear strength. An increase in shear strength for decreasing aspect ratio is generally accepted for $M/VL < 1$. Let $M = VH + M_a$ where M_a is a flexural moment on top of the wall and H is the wall height; for slender walls $H/L > 1$ to have $M/VL < 1$ they must have a moment M_a on top of the wall in opposite direc tion to the moment produced by the shear force ($M_a < 0$). This moment produce a rotational rest rain on top of wall. The presence of M_a can be seen as a reduction of the aspect ratio: $H_e = H/L - M_a/VL$. For squat walls, stren gth increases proportionally with decreasing M/VL. In this case M_a may be positive or negative and still have $M/VL < 1$. As before the moment may be seen to increase or decrease respectively the aspect ratio of the wall. The effect of the flexural moment M_a is interpreted as a change in aspect ratio. No description of the effect of the flexur al moment is included in codes for slender walls ($H/L > 1$ and $M_a > 0$) [6], [13], [14], [15]; an exception found in Peru's code [16].

Flexural moment may eventually produce tension in the wall, reducing the effective area to resist sliding shear as recognized by the Eurocode [17], however sliding shear strength is usually larger than diagonal tension shear strength [18].

The contention in this paper is th at the additio nal lateral deformation due to f lexural moment affects the magnitude of the shear cracking strength due to tension and that the effects of aspect ratio and flexural m oment need to be considered as independent variables for the prediction of shear cracking strength. A shear cracking strength prediction will be developed next.

HYPOTHESIS

It will be consider ed that c racking is due to the re lative lateral deformation of the wall, disregarding which load produced such deformation: shear or a combination of shear an moment. A linear elastic behaviour of the wa ll is assumed and no predictions will be given after the first inclined cracks due to tension app ear in th e wall. A trilinear she ar displacement model of confined masonry is shown in Fig. 1 [19]. Hereafter, V_n will be used to refer to the cracking shear load when no additional mo ment is considered on top of the wall, and V_n' to the same value after considering the effect of the moment.

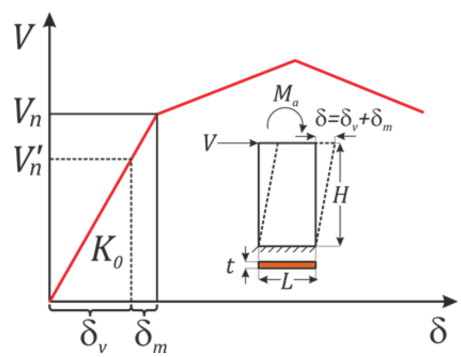

K_0 wall stiffness, δ_v, δ_m displacements due to shear force V and a flexural moment M_a, respectively

Figure 1 Model of shear–displacement envelope

Using a linear relationship between displacement and shear, and elastic theory to calculate lateral displacements due to shear load and flexural moment, equations 1 and 2 can be written:

$$V_n' = V_n - \delta_m K_0 = V_n - \frac{M_a}{H_k}, \qquad H_k = \frac{2}{3}\frac{k_f + k_v}{k_v} H \tag{1}$$

where:

$$\delta_m = \frac{M_a\, H^2}{2\, EI}, \quad K_0 = \frac{k_f k_v}{k_f + k_v}, \quad k_f = \frac{3EI}{H^3}, \quad k_v = \frac{GA}{\kappa H}, \quad I = \frac{tL^3}{12}\ , \ A = tL \tag{2}$$

where E, G are masonry's modulus of elasticity and shear modulus respectively, κ the shear factor, L and H are the total length and height of the wall. Using normalized parameters, $w = H/L$, $M_a = \beta V_n' H/2$ and $\eta = G/E$, the quotient of the cracking shear force considering and without considering the effect of a flexural moment M_a on top of the wall $\alpha = V_n'/V_n$ may be written as

$$\alpha = \frac{1}{1 + \frac{15\beta\eta w^2}{20\eta w^2 + 6}} \tag{3}$$

Parameter β is convenient as it represents the amout of flexural moment, and depending on its value, several conditions may be readily identified: if $\beta = -1$ the wall has its upper end rotationally restrained, if $\beta = 0$ the wall is in cantilever and otherwise the wall undergoes a fixed rotation of its top, larger than that of a cantilever.

As it should, Ec. (3) predicts no effect if there is no moment applied i.e. $\beta = 0$ imply $\alpha = 1$, and when moment is applied in opposite direction to the moment generated by the shear force ($\beta < 0$) an increase on cracking strength is predicted ($\alpha > 1$). Meli [7], described this effect in terms of aspect ratio for tests conducted restraining the rotation of the top of the wall, tests known as diagonal compression tests; here, the effect of moment and aspect ratio are clearly separated. α increases with $\eta = G/E$, as when η increases shear deformation is reduced, increasing the ratio of flexural to shear deformation; consequently, the effect of moment is more pronounced.

EXPERIMENTAL PROGRAM

Four full scale confined masonry walls were built and grouped into two sets *M1* and *M2* with two identical specimens 'a' and 'b' each. Specimen 'a' in, each set was used as a reference, loaded with cycles of increasing shear force only, while wall 'b' in each set were tested with cyclic shear force and moment on its top. Walls in set *M1* were built with hand-made solid clay bricks 234×118×53 mm while for walls in set *M2*, extruded multi-perforated clay bricks 241x116x60 mm were used. Mortar 1:3 cement to sand ratio was used for the joints in both sets. Tie-column and tie-beam longitudinal and transverse reinforcement for each set is specified in Fig. 2, no horizontal reinforcement was used. Specimens were designed and constructed following the requirements of the Mexican Building Code [20] and were reinforced to procure shear failure. All the specimens were constructed on top of reinforced concrete foundation beams.

Masonry compression strength f_m and masonry modulus of elasticity E_m were obtained from compression tests of masonry piles and shear modulus G_m from diagonal compression test. Similarly, concrete compression strength f_c' and corresponding modulus of elasticity E_c were obtained with standard ASTM tests. Average values are shown in Table 1.

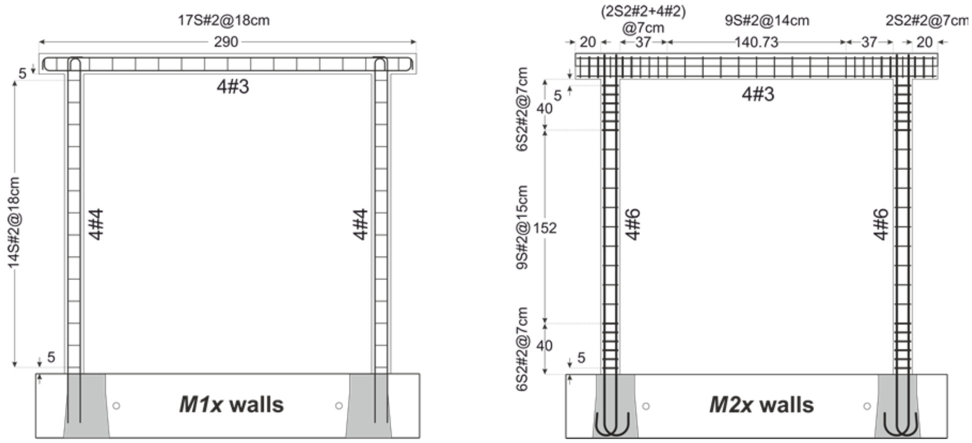

Figure 2 Wall reinforcement for specimens in set *M1* and *M2*

Table 1 Material properties

	f_m (MPa)	v_m (MPa)	E_m (MPa)	G_m (MPa)	f_c' (MPa)	E_c (MPa)	f_y (MPa)	E_s (MPa)
$M1a$	4.45	0.31	623.11	171.52	23.24	10352.68	404.13	205998
$M1b$	10.76	0.41	4136.38	586.22	10.48	8259.26	395.89	197940
$M2a$	4.53	0.33	785.51	139.65	21.28	8088.33	404.13	205998
$M2b$	9.09	0.45	3739.06	586.22	10.72	9303.46	395.89	197940

TEST SETUP AND LOAD SEQUENCE

Lab setup used to apply lateral load, vertical load and bending moment is depicted in Fig. 3. Lateral load was distributed in the wall by means of a steel beam fastened to the slab with 22.2 mm diameter bolts arranged symmetrically relative to the plane of the specimen. Two vertical actuators, located at each side of the wall, were used to apply the vertical and flexural loads. For walls in set *M2* (*M2x*) a third actuator was used, located at the central part of the wall, to also apply axial load; the aim was to achieve a more uniform vertical load on the wall.

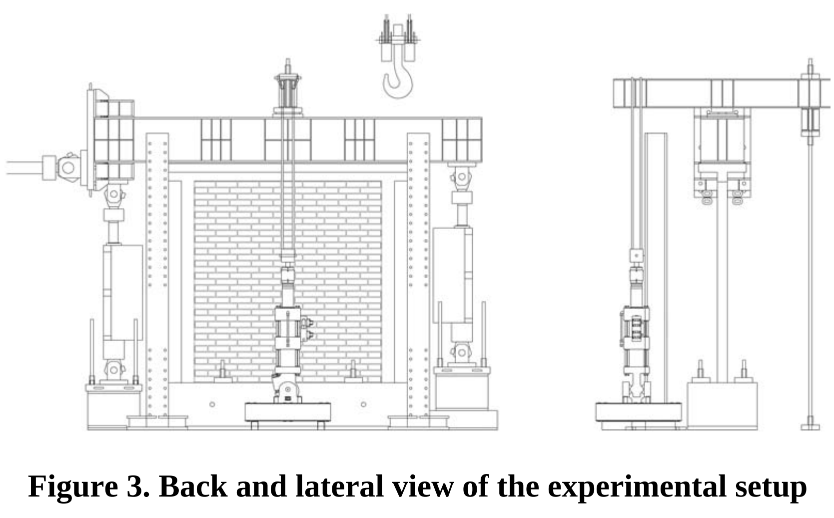

Figure 3. Back and lateral view of the experimental setup

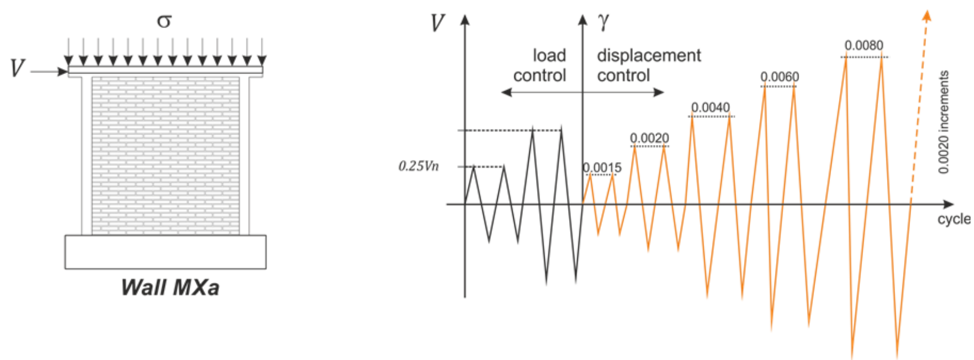

Figure 4 Load sequence for *MXa* specimens

To simulate the effect of gravity loading, a constant compressive stress equal to $\sigma = 1.32\ MPa$ ($P_a = 392\ kN$), for $M1x$ walls and $\sigma = 1.74\ MPa$ ($P_b = 490\ kN$), for $M2x$ walls, was applied. For the reference walls, labelled as 'a' in each set (*MXa)* no bending moment on top of the wall was induced. The vertical load was applied first followed by pairs of load controlled cycles with peak shear loads equal to 0.25 V_n and 0.5 V_n, as shown in Fig. 4, where V_n is the nominal shear strength according to the Mexican code [20]

$$V_n = 0.5 v_m A_T + 0.3P \leq 1.5 v_m A_T \tag{4}$$

Afterwards the sequence changed to displacement control, applying pairs of cycles with increasing peak deformations $\gamma = \delta/H =$ 0.0015, 0.002, 0.004, 0.006, 0.008, etc. The test stopped when a 20% decrease in shear strength was measured for a peak displacement or the wall failed. Moment was also applied on top of *MXb* walls. During the load controlled sequence, cycles with peak values reaching $(0.25V_n, 0.5M_a)$ and $(0.5V_n, M_a)$ were applied. For the displacement controlled cycles the bending moment was applied linearly increasing with displacement up to M_a when the lateral drift reached 0.0012 (3 mm) for specimen *M1b* and 0.0014 (3.6 mm) for specimen *M2b*. Similarly when unloading, moment M_a was maintained until the value of deformation came down to 0.0012 or 0.0014, depending on the wall, when it started to decrease linearly with deformation towards the negative branch of the cycle. The intention was to assure that the desired level of moment was attained before the first diagonal cracks due to shear appear. (See Fig. 5).

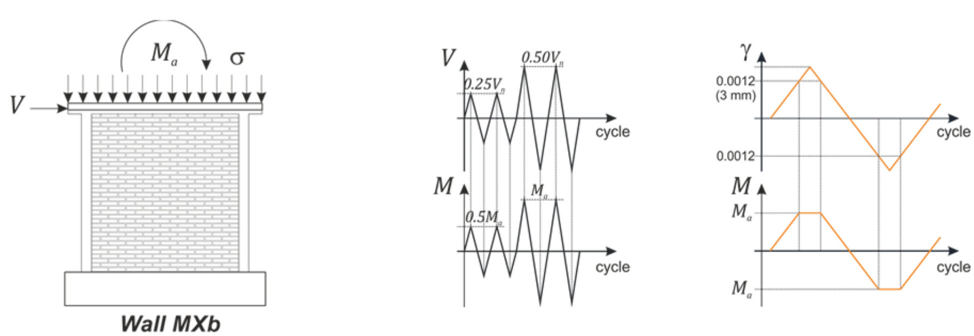

Figure 5 Load sequence for *MXb* specimens

This procedure allows knowing at every step of the test the value of the applied moment; however, the shear load applied can, at best, be estimated. A load sequence that keeps the relation M/V constant requires a more complex control procedure that adjusts the applied moment based on the lateral load feedback, keeping the lateral load and moment as a dependent on displacement. The first scheme was selected as it is simpler to implement. However, for the wall $M2b$ the moment applied during the loading branch, produced lateral displacements larger than that required in the displacement controlled command. As a result, a lateral load in opposite direction to the displacement generated by the moment was required to achieve the target displacement. In Fig. 6 the load sequence for wall $M2b$ is depicted. Starting with cero lateral displacement and cero lateral load (between points B and C in the corresponding curve) a target displacement is specified to the control system to reach point C, which is 0.0014·H. As explained above, the moment is, at the same time, increased proportionally up to M_a. The displacement produced by the moment is larger than required; consequently, a negative lateral load was applied by the control system to reduce such displacement. Next target displacement is point D and the moment is maintained constant, the lateral load reduces its absolute value eventually turning it into a positive force (in the same direction that the target displacement). A similar phenomenon can be observed while unloading.

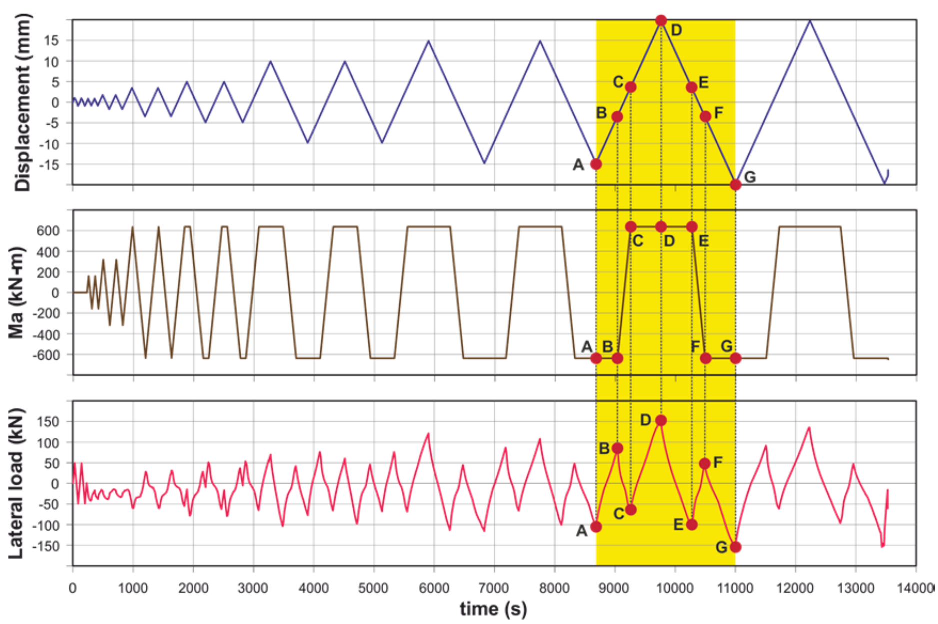

Figure 6 Load sequence of wall *M2b*

CRACK PATTERNS

Final crack patterns for all specimens are shown in Fig. 7. *M1a* and *M1b* walls show inclined shear cracks due to tension; however, *M1b*'s cracks are more distributed and a greater number of smaller cracks can be observed. *M1b*'s south tie-column shows initiation of crushing of its cover attributed to the additional bending moment.

M2a and *M2b*'s crack patterns show more differences. *M2a*'s crack pattern is similar to that of wall *M1a* typical of walls with damage dominated by shear. The added transverse reinforcement at the ends of the tie-columns was responsible of the fan of small cracks in the upper end of

M1a's south tie-column. The extra reinforcement delayed the complete penetration of the tie-column by a single crack, as is usually the case. Wall *M2b* shows a more complex crack pattern, with a combination of horizontal and inclined racks. Many horizontal cracks can be observed in the wall and all along the tie-columns due to flexure. Shear cracks due to tension showed in a more distributed pattern as in the case of *M1b*. It was also evident in *M2b*, a vertical crack running along the interface between the tie-columns and the wall indicating separation of the tie-columns from the wall. Failure of *M2b* was finally reached when the north tie-column buckled.

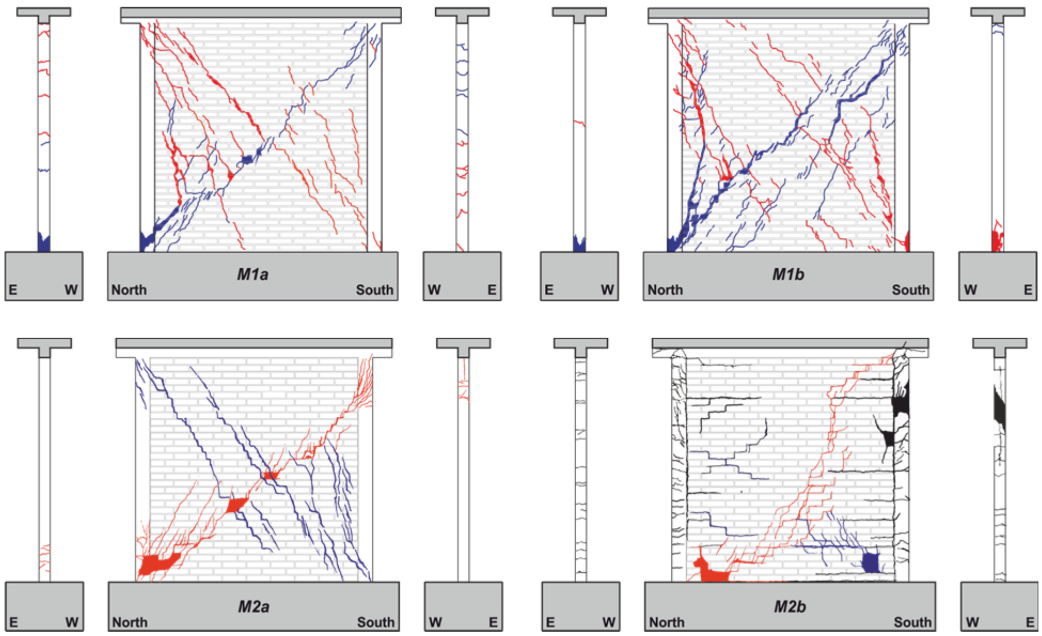

Figure 7 Final crack patterns *M1x* and *M2x* series

HYSTERESIS CURVES AND ENVELOPES

The hysteresis curves are shown in Fig. 8. Dashed red lines are used to mark the deformation used to stop/start the variation of moment. Broader hysteresis cycles can be observed for wall *M1b* as compared to those of *M1a*, revealing the effect of the applied flexural moment and indicative of a larger amount of energy being dissipated. *M1b*'s cycles are apparently more stable, as the shapes of the cycles for the repetition of the load tend to be very similar in *M1b*, while in *M1a* larger variations on the shape of the cycles can be observed. The unusual hysteresis curve for *M2b* is a consequence of the load sequence used. As it was explained above, negative forces developed when displacements due to flexure in the positive direction exceed the target displacement, and similarly when unloading.

Envelopes for the hysteresis curves are presented in Fig. 9 and their critical points are summarized in Table 2. In both sets of walls a marked reduction of the cracking strength can be observed when a moment is applied on top of the wall as compared to the corresponding reference specimen. The reduction is in good agreement with the proposed prediction as will be seen later.

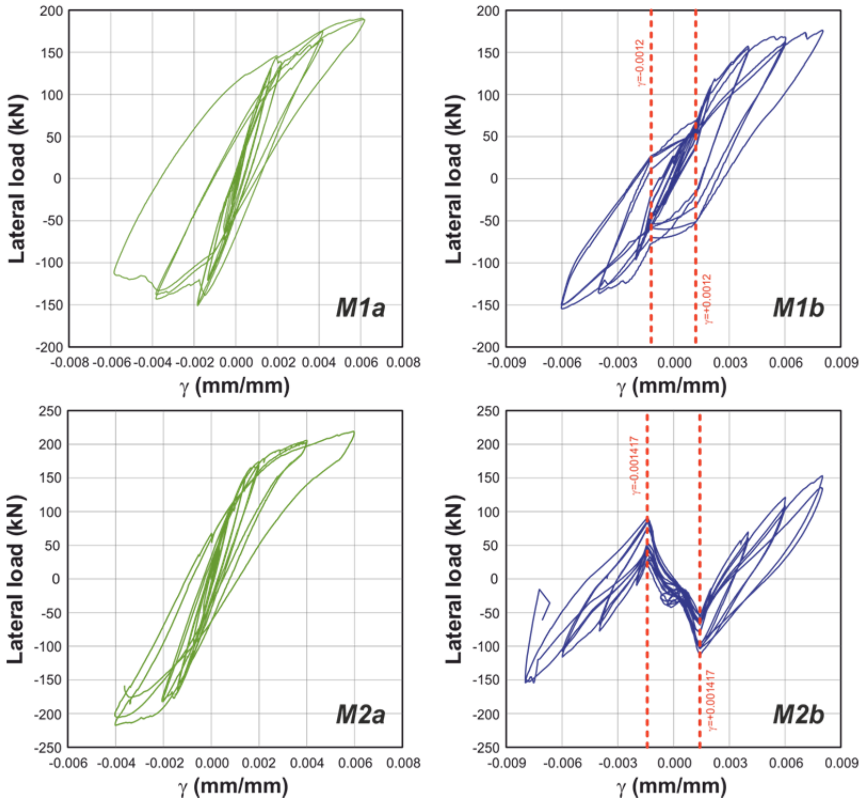

Figure 8 Hysteresis curves

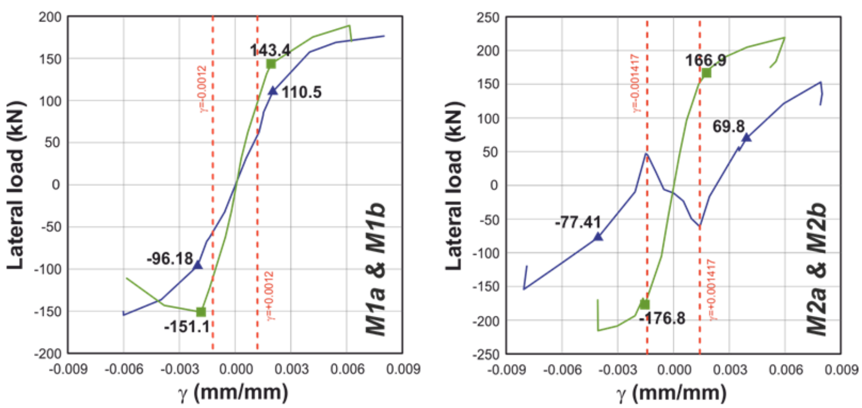

Figure 9 Envelopes of hysteresis loops

Table 2. Critical points values

Wall	Cracking				Strength				Ultimate			
	V_c^+ (kN)	d_c^+ (mm)	V_c^- (kN)	d_c^- (mm)	V_{max}^+ (kN)	d_{max}^+ (mm)	V_{max}^- (kN)	d_{max}^- (mm)	V_u^+ (kN	d_u^+ (mm)	V_u^- (kN)	d_u^- (mm)
M1a	143.4	4.75	-151.1	-4.50	188.9	15.12	-151.1	-4.50	170.2	15.37	-111.0	-14.32
M1b	110.5	4.97	-96.2	-4.94	176.4	19.62	-154.7	-14.72	176.4	19.62	-150.5	-14.76
M2a	166.9	4.39	-176.8	-3.80	219.1	14.8	-215.5	-10.04	175.0	12.87	-170.0	-10.07
M2b	69.8	9.70	-77.4	-10.04	153.2	19.58	-154.2	-19.92	119.4	19.51	-119.8	-19.50

The stiffness of wall *M1b* is smaller than that of *M1a*, as the lateral displacements of wall *M1b* are due to shear force and bending moment, so, clearly, the same lateral displacement is reached with a smaller shear force. When the moment stopped to increase, as marked by the dashed line, there is a sudden stiffness increase; being then much similar to that of *M1a*, as only the lateral load is changing. (See *M1b* curve from the dashed line towards 110.5 kN in the positive branch and towards -96.21 in the negative branch). In both the positive and negative branches of *M1b* cracking occur after M_a was attained as expected. (i.e after the dashed line).

In set *M2* the difference in shear cracking strength between *M2b* and *M2a* is more pronounced as compared to set *M1* (in the positive branch from 166.9 kN in *M2a* to 69.8 kN in *M2b*, and in the negative branch from -176.8 kN to -77.4 kN), due to the large moment applied to *M2b*. The displacement at which the cracking strength was reached for *M2b* was larger than for *M2a*; however, during the test some rigid body rotations of the wall were detected, mainly due to slippage of the concrete conic block where the longitudinal reinforcement of the tie columns were anchored. The small base rotations in *M2b* generated amplified lateral displacements on its top, making it impossible a direct comparison of *M2b*'s lateral displacements with those of the reference wall *M2a*. In any case, the formula for the prediction of the cracking strength assumes elastic displacements due to shear and flexure. However, for large moments on top of the wall, like the ones applies to *M2b* the neutral axis of the wall section may well be inside the wall. In that case displacements can no longer be assumed linear. Nonetheless, the deduced expression may still give accurate predictions as will be seen in the next section.

The shear strength was also reduced in both sets when moment is applied on top of the wall, in the same direction of the moment due to shear; however, the prediction of this reduction is outside the scope of the used theory.

SHEAR-MOMENT INTERACTION

In order to have a realistic value of the nominal shear force, it was directly obtained from the cracking shear force of the reference walls *M1a* and *M2a* tested without moment, instead of using the results from the diagonal compression tests of masonry assemblages to compute is value with a code´s formula. Once the tests were done, $\alpha = V_n'/V_n$ was evaluated. Table 3 collects both, the calculated and measured values needed to establish the comparison.

Table 3 Comparison of experimental and theoretical results

	M1a	*M1b*	*M2a*	*M2b*
M_a (kN-m)	0	176.5 0 637.4		
P (kN)	392.3	392.3 490.3 490.3		
V_n (kN)	143.6	143.6 171.9 171.9		
V_n'		110.5 73.60		
$\beta = M_a/(V_n'H/2)$	0	1.3 0		7.01
α (calculated)	1.0	0.71 1.0 0.42		
α (experimental)	1.0	0.77 1.0 0.43		

The predicted value is given by Equation (3); the aspect ratio was nearly equal to 1 in both sets, $w_1 = 0.9921$ for set *M1* and $w_2 = 0.9722$ for set *M2*, Average $\eta = G/E$ was obtained from the material tests and $\beta = M_a/(V_n'H/2)$. Using the previous parameters the theoretical value of α was computed. The relative error of the prediction was 7.79% ($e_1 = \frac{0.71-0.77}{0.77} \times 100 = 7.79$) for set *M1* and 2.11% ($e_2 = \frac{0.43-0.42}{0.42} \times 100 = 2.11$) for set *M2* which is in good agreement with the theoretical expressions.

CONCLUSIONS

Based on the results of the tests and their comparison to the analytical predictions the following conclusions may be drawn:

- The presence of flexural moment on top of the wall affects the magnitude of the shear force that produces the first inclined cracks due to tension in a confined masonry wall: i.e. shear cracking strength is not independent from the level of flexural moment.

- The hypothesis in which the lateral deformation at cracking is the same whether it was caused by a lateral load or a lateral load and moment was satisfied to a reasonable level of accuracy in *M1* series, only 4.6% deviation in the positive branch and 9.8% of deviation in the negative branch. However, because both walls initiated cracking in the positive branch, the former value is considered more representative, while the larger deviation in the negative branch, may be attributed, in part, to nonlinear effects, as some damage in the wall was present and not considered in the developed theory. Cracking in set *M2* walls occurred at different levels of displacement due, in part, to rigid body rotations in *M2b*, so, the hypothesis can't be substantiated.

- The reduction of the shear force that produced diagonal tension cracks was estimated with good accuracy, with the proposed formula. The proposed expression separates the effect of moment and aspect ratio.

- Ductilities defined herein as displacements at peak strength and ultimate strength divided by the displacement at cracking, which is also considered a limit of the elastic range, increased when displacements were produced by shear force and moment, as compared with those obtained with shear forces only.

- The presence of flexural moment in a wall should explicitly be considered to estimate the shear strength of the wall. Although no predictions are made here for the shear strength of the wall, the experimental results presented here show that the shear strength is also affected by the flexural moment.

ACKNOWLEDGEMENTS

The investigation was supported by the Federal District Government (GDF) grant No CT/04/10 and partially by the National Council for Science and Technology (CONACYT) Grant No 133225. The tests were conducted at the Structures Lab of the Institute of Engineering (UNAM) with Eddy Grandry† and Yussef as control technicians and support personnel of the Lab, Raymundo, Salomon, Ismael and Agustin.

REFERENCES

1. Riahi, Z., Elwood, K.J. and Alcocer, .S.M. (2009) “Backbone Model for Confined Masonry Walls for Performance-Based Seismic Design”, Journal of Structural Engineering, 135,644-654.
2. Hernández, O. and Meli, R. (1976) “Modalidades de Refuerzo para Mejorar el Comportamiento Sísmico de Muros de Mampostería No 382”, México, D.F., Instituto de Ingeniería, UNAM.
3. Confined Masonry Network (2011) “Siesmic Design Guide for Low-Rise Confined Masonry Buildings”, World Housing Enciclopedia , EERO & IAEE.
4. Alcocer, S. and Meli, R. (1995) “Test Program on the Seismic Behaviour of Confined Masonry Walls”, The Masonry Society Journal (Boulder), 12:2, 68-76.
5. NSR-10 (2010) “Reglamento Colombiano de Construcción Sismo Resistente”, Bogotá, D.C., Colombia, Ministerio de Ambiente, Vivienda y Desarrollo Territorial.
6. NZS (2004) (4230:2004) “Design of Reinforced Concrete Masonry Structures”, Wellington: Standards Association of New Zealand.
7. Meli, R. (1975) “Comportamiento Sísmico de Muros de Mampostería No 352”, México, D.F., Instituto de Ingeniería, UNAM.
8. Alvarez, J.J. (1996) “Some Topics of the Seismic Behaviour of Confined Masonry Structures”, 11th World Conference on Eartquake Engineering, Acapulco, México.
9. Zeballos, A., San Bartolomé, A., Muñoz, A. and. (1992) “Efectos de la Esbeltez sobre la Resistencia a Fuerza Cortante de los Muros de Albañilería Confinada. Análisis por Elementos Finitos”, Blog de Angel San Bartolomé, Pontificia Universidad Católica de Perú, http://blog.pucp.edu.pe/media/688/20070504-Esbeltez%20-%20Elementos%20finitos.pdf.
10. Voon, K.C. and Ingham, J.M. (2006) “Experimental In-Plane Shear Strength Investigation of Reinforced Concrete Masonry Walls”, Journal of Structural Engineering, March, 132:3,400-4008.
11. T. Kaminosono, Y. Yamazaki, M. Teshigawara and S. Okamoto (1992) “New Design Guidelines for Medium Rise Reinforced Masonry Buildings in Japan”, Earthquake Engineering, 10th World Conference on Earthquake engineering, Madrid, Spain.
12. Fattal, S.G. and Todd D.R. (1991) “Ultimate Strength of Masonry Shear Walls: Predictions vs Test Results NISTIR 4633”, National Institute of Standards and Technology.
13. MSJC SD (2002) TMS 402-08/ACI, 530-08/ASCE 6-08, “Building Code Requirements and Specification for Masonry Structures”, Masonry Standards Joint Committee.
14. UBC SD (1997) “Uniform Building Code”, Whittier, California: International Conference of Building Officials.
15. CSA (2004) S304.1-04 “Design of Masonry Structures”, Mississauga, Ontario, Canada: Canadian Standard Association.
16. E.070 (2006) “Norma Técnica E.070 Albañilería”, Perú.
17. EC6 (2002) “Eurocode 6: Design of Masonry Structures - Part 1-1: Common Rules for Reinforced and Unreinforced Masonry Structures”, European Standards.
18. Tomazevic, M. (2009) “Shear Resistance of Masonry Walls and Eurocode 6: Shear Versus Tensile Strength of Masonry”, Materials and Structures, 42. 889-907.
19. Flores, L.E. and Alcocer, S.M. (1996) “Calculated Response of Confined Masonry Structures”, 11th World Conference on Earthquake Engineering, Acapulco, México.
20. NTCM (2004) “Normas Técnicas Complementarias para Diseño y Construcción de Estructuras de Mampotsería”, Mexico: Gobierno del Distrito Federal (in Spanish).